Prediction of Cement Physical Properties by Virtual Testing

by

D.P. Bentz[a], C.J. Haecker[b], X.P. Feng[a] and P.E. Stutzman[a]
[a] Building and Fire Research Laboratory
National Institute of Standards and Technology
Gaithersburg, MD 20899 USA

[b] Wilhelm Dyckerhoff Institute
Wiesbaden, GERMANY

Reprinted from Process Technology of Cement Manufacturing. Fifth International VDZ Congress. Proceedings. Düsseldorf, Germany, September 23-27, 2002, pp. 53-63, 2003.

NIST
National Institute of Standards and Technology
Technology Administration, U.S. Department of Commerce

PREDICTION OF CEMENT PHYSICAL PROPERTIES BY VIRTUAL TESTING

D.P. Bentz[a], C.J. Haecker[b], X.P. Feng[a], and P.E. Stutzman[a]
[a]National Institute of Standards and Technology, 100 Bureau Drive Stop 8621, Gaithersburg, MD 20899-8621 USA
[b]Wilhelm Dyckerhoff Institute, Wiesbaden, GERMANY

ABSTRACT

Assuring the quality of the massive quantities of cement produced worldwide each year is a daunting task. Currently, the cement industry performs extensive physical testing to assess the quality of their product, resulting in large costs for both materials (and their disposal) and labor. One of the major goals of the Virtual Cement and Concrete Testing Laboratory (VCCTL) consortium is to provide the technology to reduce the number of necessary physical tests. In this paper, the ability of the VCCTL to successfully predict a wide variety of cement paste physical properties is demonstrated. Predicted physical properties are compared to experimental measurements for degree of hydration, heat of hydration, chemical shrinkage, setting times, compressive strength development, and pore solution concentrations. When the starting materials are characterized in detail, good agreement is exhibited between VCCTL model predictions and experimental measurements, highlighting the potential for this virtual technology to ultimately save the cement industry both time and money.

Introduction

To produce high quality long lasting concrete structures, cements of a high and consistent quality must be employed. Worldwide, the cement industry spends countless hours assuring the quality of its products, mainly based on laboratory tests. In the USA, most physical testing of cements is performed according to ASTM standards /1/; in Germany, testing is generally governed by the European Norm /2/. Technologies that could reduce the number of physical tests needed for cement production (and optimization) would clearly be a welcome addition. One such potential technology is the use of virtual testing. In virtual testing, starting materials are characterized and their performance predicted via the use of computer models. This should result in savings in both resources (materials, labor, etc.) and time, as 28 d performance can be simulated in just a few hours of computer time. An additional benefit of virtual testing is the capability to perform a large number of “what-if” type computations to explore new material systems and optimize existing ones, e.g., what is the optimum sulfate content and form for a particular cement or how will the performance of a cement change if its Blaine fineness is increased by 10 m^2/kg?

To address this goal of reducing the necessary physical testing of cement and concrete, in January 2001, the Virtual Cement and Concrete Testing Laboratory (VCCTL) consortium was formed. The consortium is a U.S. government/industry collaboration headquartered in the Building and Fire Research Laboratory at the National Institute of Standards and Technology (NIST). At NIST, the Information Technology Laboratory and the Materials Science and Engineering Laboratory also participate in the consortium's research projects. Current industrial members of the consortium include: Cemex, Dyckerhoff Zement GmbH, Holcim Inc., Master Builders Technologies, the Portland Cement Association, Verein Deutscher Zementwerke E.V. (the German Cement Association), and W.R. Grace & Co. - Conn. Version 1.0 of the VCCTL software is available to the general public at http://vcctl.cbt.nist.gov. A user's manual /3/ is available online as menu selection 0 from the main VCCTL menu. In this paper, the VCCTL will be applied to predicting a variety of physical properties of cement pastes to illustrate its potential usefulness to the cement industry.

Experimental Procedure

To illustrate the predictive capabilities of the VCCTL, two cements distributed by the Cement and Concrete Reference Laboratory (CCRL) were utilized /4,5/. Twice each year, the CCRL sends out proficiency samples of two cements for evaluation by laboratories throughout North America and 22 other countries. Proficiency samples of CCRL cements 135 and 141 were obtained in January of 2000 and June of 2001, respectively. The samples were provided double-sealed in plastic bags in cardboard boxes. Samples of the two cement powders were subsequently analyzed with respect to particle size distribution (PSD) and by scanning electron microscopy (SEM) and X-ray microanalysis. This characterization provides the inputs needed by the VCCTL for the detailed simulation of hydration and microstructure development.

Particle Size Distribution

The particle size distributions of CCRL cements 135 and 141 were determined using laser diffraction techniques at the laboratories of Dyckerhoff Zement in Germany. For the measurements, a HELOS instrument type RODOS T4.1 from

SYMPATEC GmbH, Germany[1] was used. The focal distance of the HELOS instrument was set at 87.5 µm, allowing the measurement of particles with diameters between 0.25 µm and 87.5 µm.

The measuring time varied between 10 s and 30 s per sample. The average PSD curves for each cement are shown in Figure 1. The PSDs measured for the two cements are seen to be quite similar, as are their Blaine finenesses (cement 135: 394 m^2/kg and cement 141: 397 m^2/kg) as measured via the standard ASTM C204 technique /1/ in the CCRL testing program /4,5/. These measured PSDs are used as one direct input into the VCCTL software.

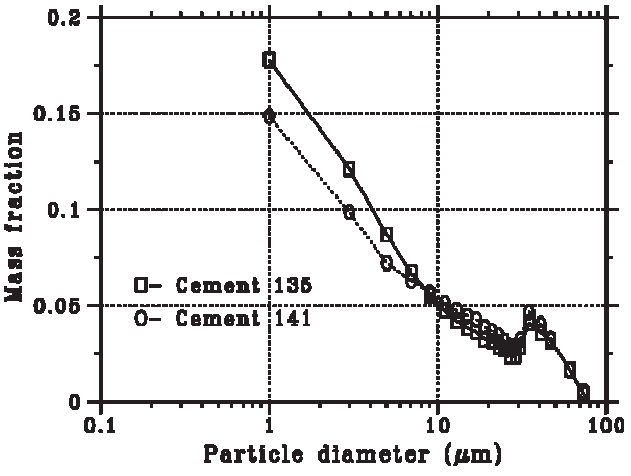

Figure 1

Scanning Electron Microscopy Imaging

The sample preparation techniques for samples to be analyzed using SEM have been described in detail elsewhere /6,7/, but will be briefly reviewed here. To prepare a polished specimen for viewing in the SEM, approximately 25 g of the powder to be imaged is blended with an epoxy resin to form an extremely viscous paste. The resin/powder mixture is pressed into a small cylindrical mold and cured at 60 °C for 24 h. The cured specimen is then cut to obtain a plane surface for imaging.

Saw marks are removed by grinding with 400 grit followed by 600 grit sandpaper. Final polishing is done on a lap wheel with (6, 3, 1, and 0.25) µm diamond paste for 30 s each. After each polishing, the specimen is cleaned using a clean cloth. After the final polishing step, ethanol is used to remove any residual polishing compound. The final polished specimen is coated with carbon to provide a conductive surface for viewing in the SEM.

Once properly prepared, the specimen is placed in the SEM viewing chamber, and signals are collected for the backscattered electrons and X-rays. Typical accelerating voltage and probe current for the backscattered electron images are 12 kV and 2 nA, respectively. For the X-ray images, the probe current is increased to about 10 nA. For analysis of cement powders, in addition to the backscattered electron signal, X-ray images are collected for Ca, Si, Al, Fe, S, K, and Mg. Because these X-ray images are collected at the same location as the backscattered electron image, this series of images can be combined to determine the mineral phase present at each location (pixel) in the two-dimensional image (typically 512 pixels by 400 pixels in size). Typically, magnifications of 250x or 500x are employed for obtaining the SEM and X-ray images.

To process the input SEM/X-ray images and to determine the distribution of phases, a decision tree is traversed for each pixel location in the images. An example of a decision tree for a typical cement powder is shown in Figure 2. In this figure, X^* represents a critical threshold greylevel value. Pixels having a greylevel greater than the value of X^* are considered to contain the element of interest and those with a greylevel below X^* are classified as not containing the element. To determine the values of X^* for each element, the corresponding greylevel histogram /8/ for each X-ray image is viewed.

[1] Certain commercial equipment is identified in this report to specify the experimental procedure. In no case does such identification imply endorsement by the National Institute of Standards and Technology, nor does it indicate that the equipment is necessarily the best available for the purpose.

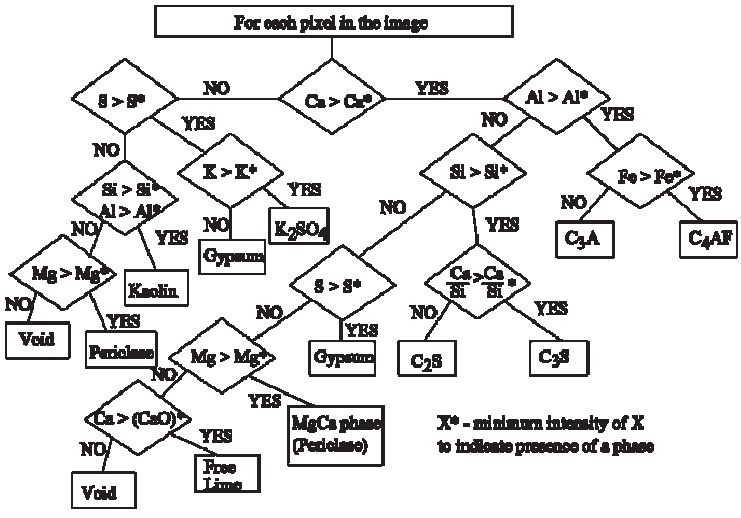

Figure 2

After the segmentation tree is traversed, the segmented image produced will still contain a substantial amount of random noise. To improve the image quality, three “filters” are applied in succession to the processed image. First, all isolated one pixel “solid” pixels are converted to porosity. Second, all isolated one pixel “pores” (totally surrounded by solids) are converted to the majority surrounding solid phase. Finally, a median filter /8/ is applied to replace each solid pixel by the majority solid phase present in the surrounding neighborhood, typically a centered 5 pixel x 5 pixel square. This three-fold process removes the remaining noise present in the segmented image, producing an image ready for quantitative stereological analysis, such as those shown in Figures 3 and 4 for cements 135 and 141, respectively. For both cements 135 and 141, two separate image composites were acquired and processed in this manner. These and images for a variety of other cements are available in an online cement images database available as part of the VCCTL. The database is directly available for viewing as menu selection 1 from the main VCCTL menu.

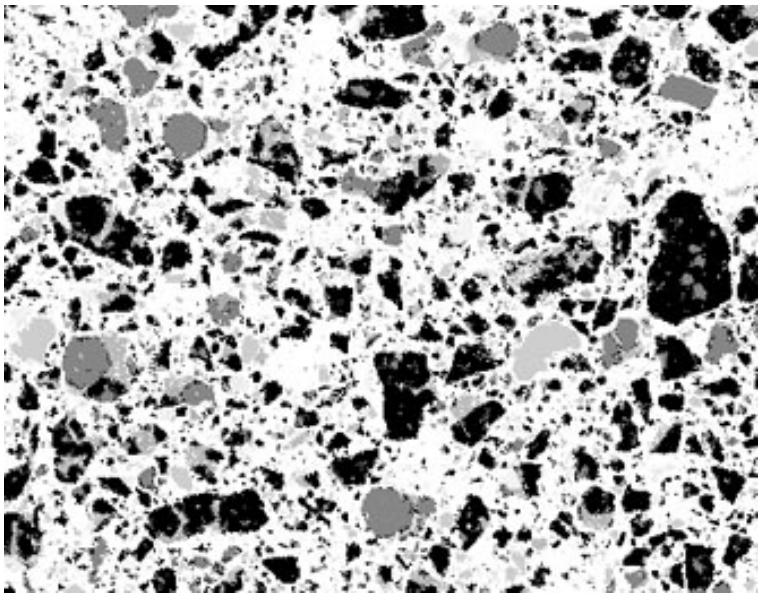

Figure 3

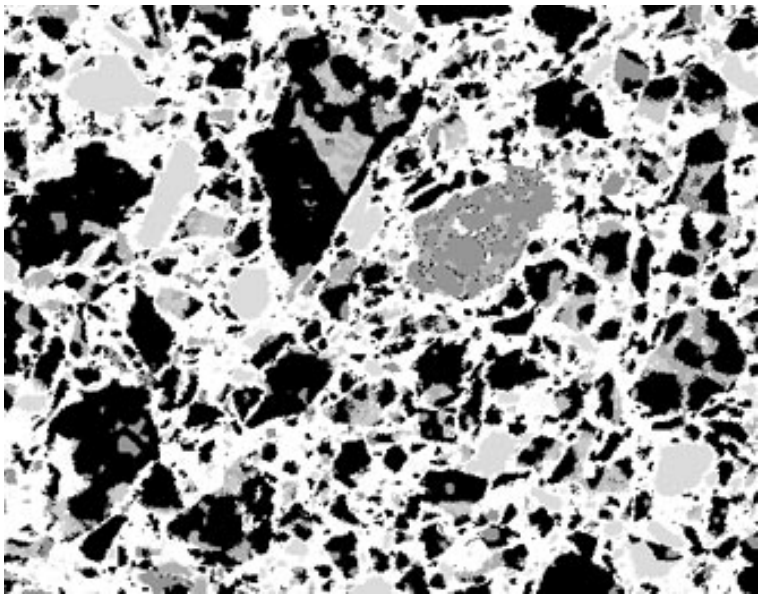

Figure 4

Mathematical Analysis of Cement Images

The final processed images can be analyzed to determine any number of stereological parameters. For cement hydration, parameters of interest include phase area fractions and phase surface perimeter fractions. For an isotropic system, the area fraction of a phase present in a 2-D image will directly correspond to its volume fraction in three dimensions. Similarly, a phase's share of the total perimeter (solid pixels in contact with porosity) will correspond to its share of the total surface area in 3-D. The surface area fractions of the phases are particularly important for cement hydration as the hydration reactions with water occur at the surfaces of the particles.

For an isotropic material, the spatial correlation functions are identical in two and three dimensions, simply being a function of distance, r. Thus, the measured 2-D correlation function for a phase or a combination of phases can be used to reconstruct a 3-D representation of the cement particles /9/. For an MxN image, the two-point correlation function for a phase, S(x,y), is determined as:

$$S(x.y) = \sum_{i=1}^{M-x} \sum_{j=1}^{N-y} \frac{I(i,j) * I(i+x, j+y)}{(M-x) * (N-y)} \qquad (1)$$

where I(x,y) is one if the pixel at location (x,y) contains the phase(s) of interest and 0 otherwise. S(x,y) is easily converted to

S(r=$\sqrt{[x^2+y^2]}$) for distances r in pixels /10/. Because the correlation function implicitly contains information on the volume fraction and specific surface of the phase(s) being analyzed, this function can be employed to reconstruct a three-dimensional representation of the cementitious particles that matches the phase volume and surface area fractions and correlation structure of the 2-D final SEM image. These starting 3-D structures of cement particles in water can then be used as input images for the cement hydration and microstructure development computer model in the VCCTL /9,10/.

The phase compositions estimated using the SEM and image analysis are compared to those calculated based on the cement oxide composition using ASTM C150 /1/ in Tables 1 and 2. For both cements 135 and 141, the SEM-measured values for C_3S significantly exceed those calculated using ASTM C150, while the values for C_2S and C_3A are generally less than those calculated from the oxide compositions. The calculations presented in ASTM C150 are known to be only approximate /11/, with quantitative optical point counting (ASTM C1356M) /1/ or X-ray diffraction (ASTM C1365) /1/ being preferred methods for performing quantitative phase analysis.

Phase	ASTM C150 composition	SEM analysis composition
C_3S	61.76	67.94 ± 3.88[a]
C_2S	21.48	17.14 ± 3.99
C_3A	7.81	7.03 ± 0.32
C_4AF	8.95	7.89 ± 0.42

Table 1: Potential Volumetric Phase Compositions for Cement 135

[a]Indicates standard deviation between the values determined for the two images.

Phase	ASTM C150 composition	SEM analysis composition
C_3S	60.59	68.3 ± 0.1
C_2S	18.14	12.32 ± 0.3
C_3A	13.65	11.9 ± 1.1
C_4AF	7.62	7.183 ± 1.042

Table 2: Potential Volumetric Phase Compositions for Cement 141

Experimental Measurements/Simulations at NIST

In addition to the data available from the CCRL proficiency sample testing program /4,5/, supplementary experimental measurements were performed at NIST. These included the determination of the non-evaporable water content of hydrating cement pastes to assess degree of hydration as a function of age (as described in detail in reference /12/), chemical shrinkage /9/, and pore solution composition. The latter analysis was performed using ion chromatographic analysis of pore solutions extracted from the hydrating cement pastes after various ages. For early ages on the order of a few hours, the pore solution was obtained simply by filtering about 150 g of hydrating cement paste (water-to-cement ratio of 0.4). For later ages, it was necessary to express the pore solution from the hardened cement paste using a special die and a universal testing machine, based on the methodology developed by Longuet /13/. For three replicates analyzed by ion chromatography, the maximum standard deviation in the determined concentrations was less than 0.004 mol/L.

All simulations were performed using the VCCTL software. Starting images of CCRL cements 135 and 141 at the necessary water-to-cement (w/c) ratios (0.25 to 0.485) were created and hydrated for various amounts of time, depending on the specific property of interest (e.g., > 28 d for compressive strength, about 10 h for setting time comparisons). As hydration occurs in the VCCTL system, a set of output files is continuously updated to reflect the development of properties with time. These results can be easily compared to those available either from the CCRL proficiency sample testing program or the experimental measurements performed at NIST. Details on the cement hydration and microstructure development computer model used in the VCCTL can be found in references /9/ and /10/.

Results

Hydration Kinetics

Figure 5 shows the model predictions and experimental results for degree of hydration under saturated and sealed conditions for cement 135. The VCCTL does an excellent job of fitting the experimental data and in matching the observed differences between saturated and sealed curing observed at longer hydration times. Early in the hydration process, excess water is readily available, so that the water lost due to self-desiccation in the sealed specimens does not have a major influence on hydration kinetics. As the specimen ages, the amount of self-desiccated (empty) porosity becomes significant, and the hydration rate of the sealed specimens trails behind those of the corresponding saturated specimens. While not a large difference is observed for the w/c=0.4 samples investigated in this study, for lower w/c ratios (now often being employed in high-performance concretes) sealed conditions can lead to a substantial reduction in the degree of hydration (and the strength) achieved at long hydration times (e.g., > 7 d).

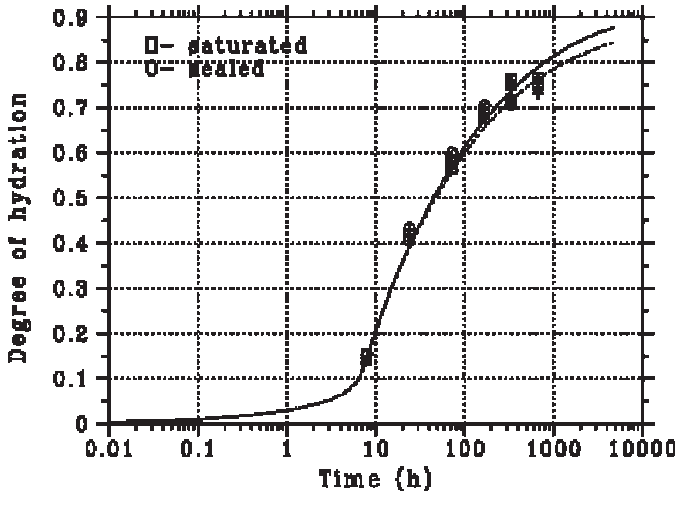

Figure 5

Figure 6 shows the equivalent plot for hydration under saturated conditions only for cement 141. While this hydration was performed at a lower temperature of 20 °C (assuming an activation energy of 40 kJ/mole for the cement hydration reactions), reasonable agreement between model and experiment is still observed, as noted previously /9/. For these two cements, the conversion factor between hydration cycles and real time is nearly a constant (0.00030 for cement 135 and 0.00035 for cement 141). These values are in good agreement with other conversion factors determined previously for CCRL cements 133 (0.00030) /10/ and 136 (0.00036) /12/.

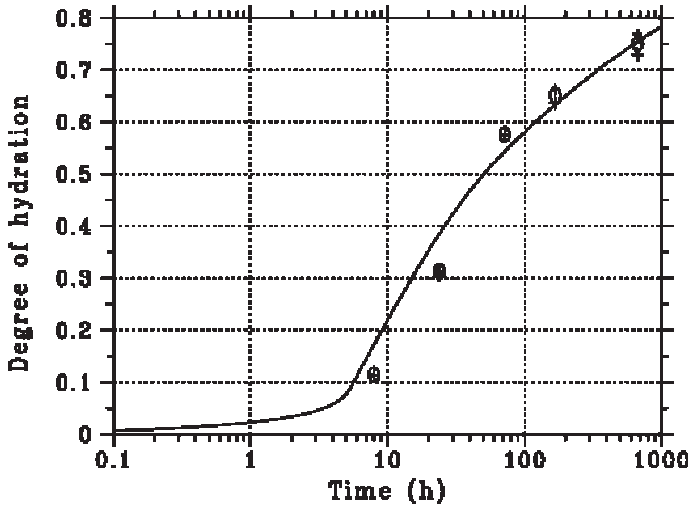

Figure 6

Heat of Hydration

The heat of hydration was determined by the testing laboratories participating in the CCRL proficiency sample testing program using the ASTM C186 heat of solution test method /1/. For this test, cement paste with w/c=0.4 was prepared and stored in sealed vials (sealed curing conditions) at 23 °C. At the time of testing, either 7 d or 28 d, the cement paste sample was digested in an acid solution and the energy released measured. By subtracting this measured value from the value determined for the starting cement powder, the heat of hydration may be determined /1/. To predict these values using the VCCTL, hydration of a w/c=0.4 cement paste under sealed conditions at 23 °C was conducted for cement 135. Table 3 provides a comparison of the values determined using the standard ASTM C186 method to those predicted by the VCCTL. At both ages, the VCCTL-predicted value is within two standard deviations of the average value determined in the

CCRL proficiency sample testing program.

Age	ASTM C186 average (J/g)	ASTM C186 standard deviation	VCCTL model prediction (J/g)
7 d	326.4	21.8	338.5
28 d	360.2	19.2	396.

Table 3: Heat of Hydration Determinations for Cement 135 (w/c=0.4)

Chemical Shrinkage

Another convenient method for monitoring hydration kinetics is via the measurement of chemical shrinkage /14/. Because the cement hydration products occupy less volume than the starting materials (cement and water), a hydrating cement paste will imbibe water in direct proportion to its ongoing hydration /14,15/. This is true except for low w/c ratio pastes (< about 0.4) where the depercolation of the capillary porosity may dramatically reduce the permeability of the cement paste and limit its imbibition rate below that required to maintain saturation during the continuing hydration /9,14/. While no standard ASTM method exists for the measurement of chemical shrinkage, a draft standard for this test is currently being considered by ASTM C01.31 subcommittee on Volume Change. The maximum expanded uncertainty /16/ in the calculated chemical shrinkage has been previously estimated /9/ to be 0.001 mL/(g of cement), assuming a coverage factor of 2 /16/.

Knowing the volume stoichiometry of all ongoing hydration reactions, it is straightforward to compute chemical shrinkage in the VCCTL cement hydration model. Figures 7 and 8 provide comparisons of model and experimental results for cements 135 and 141, respectively. Excellent agreement is observed between model and experimental results. The deviation between model and experimental results for cement 135 at later ages (> 40 h) is likely due to the depercolation of the capillary porosity mentioned above. Chemical shrinkage measurements appear to provide a rapid and convenient

method for assessing early hydration rates and may provide a simple means for evaluating cement cracking susceptibility /17/.

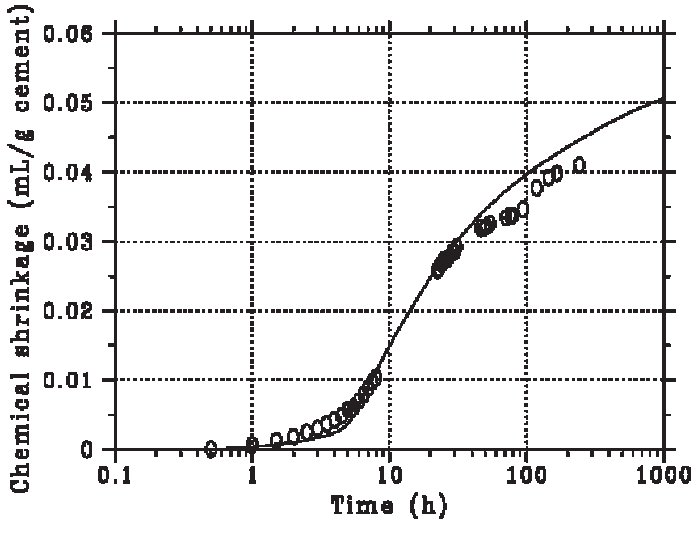

Figure 7

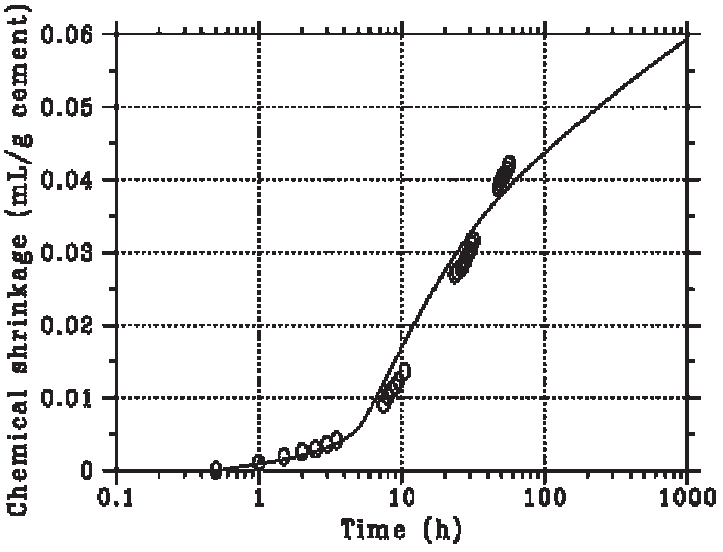

Figure 8

Setting Time Determination

One of the most important properties of a cement is its setting time, as this will regulate how much time the contractor will have to get the concrete placed and finished. In the U.S., setting times are assessed using either a Vicat (ASTM C191) or Gillmore (ASTM C266) needle /1/. These tests basically measure when the hydrating cement paste develops some finite value of resistance to penetration. Within the VCCTL software, setting is assessed using a special percolation algorithm /3,10/. The algorithm measures the fraction of total solids that are linked together by calcium silicate hydrate gel (C-S-H) and ettringite or C_3AH_6 hydration products. Thus, two touching cement particles do not comprise a percolated structure for setting unless some hydration product bridges them. In this way, the setting behavior of both well-dispersed and flocculated cement pastes can be consistently evaluated. The VCCTL returns the percolated (connected) fraction (0 to 1) for the total solids as a function of either hydration time or degree of hydration.

Figure 9 shows these percolation plots vs. time for cements 135 and 141, both hydrated at a w/c ratio determined by the ASTM Normal Consistency test (ASTM C187 /1/). The initial and final setting times determined by the Vicat and Gillmore needle tests are shown as vertical lines on the graphs as noted in the caption. The initial and final Vicat setting times are seen to approximately correspond to percolated fractions of 0.4 and 0.75, respectively. The Gillmore setting times are always slightly longer, the initial and final setting times corresponding to percolated fractions of 0.6 and 0.8, respectively.

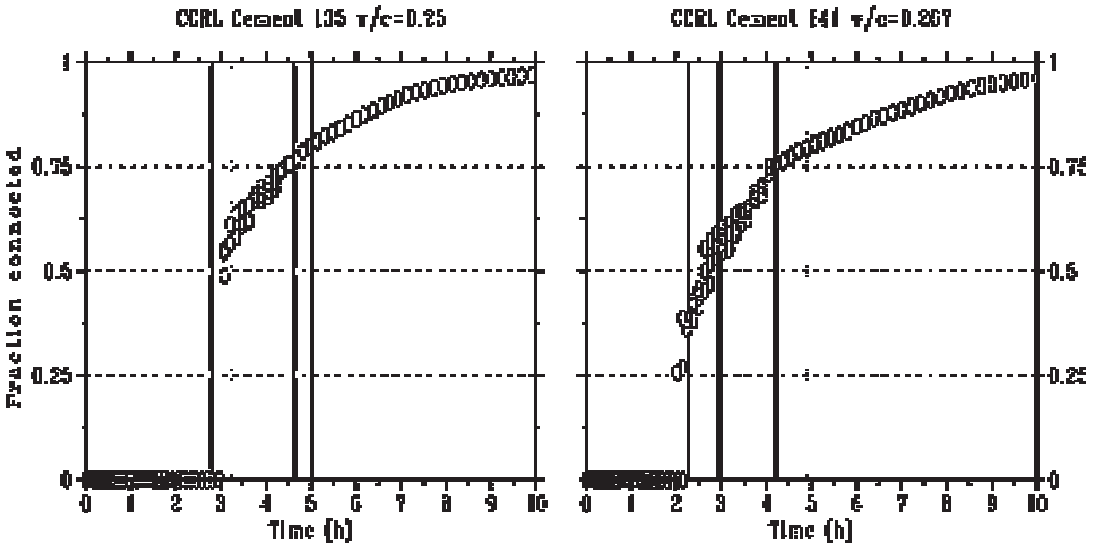

Figure 9

Pore Solution Concentrations

Some of the first year efforts in the VCCTL consortium focused on the incorporation of a module into the VCCTL software for estimating the composition of the pore solution during hydration. The new module provides estimates of the solution pH and the concentrations of the following ions: sulfate, calcium, potassium, and sodium. Based on these predicted concentrations, the conductivity of the pore solution can also be easily estimated /18/. To accurately predict the changes in pore solution composition with time, it is necessary, of course, to know both the total alkali oxide and readily soluble alkali oxide compositions of the cement (see Table 4).

Cement	Total Na_2O	Total K_2O	Readily soluble Na_2O	Readily soluble K_2O
135	0.199	0.834	0.120	0.818
141	0.405	1.04	0.250	0.860

Table 4: Alkali Contents (Mass Percentages) for Cements 135 and 141 via ASTM C114 /1/

Figures 10 and 11 show the predicted and experimental pore solution compositions in terms of the concentrations of sodium and potassium. For potassium, two predictions are provided, considering /19/ and neglecting the precipitation of syngenite (potassium calcium sulfate hydrate). Once again, good agreement between experimental observations and model predictions is seen for ages out to 1 d. The deviation between model and experiment for cement 135 at later ages (> 100 h) is likely due to some drying of the sealed specimens, reducing the saturation of the specimen and hence significantly increasing the ionic concentrations.

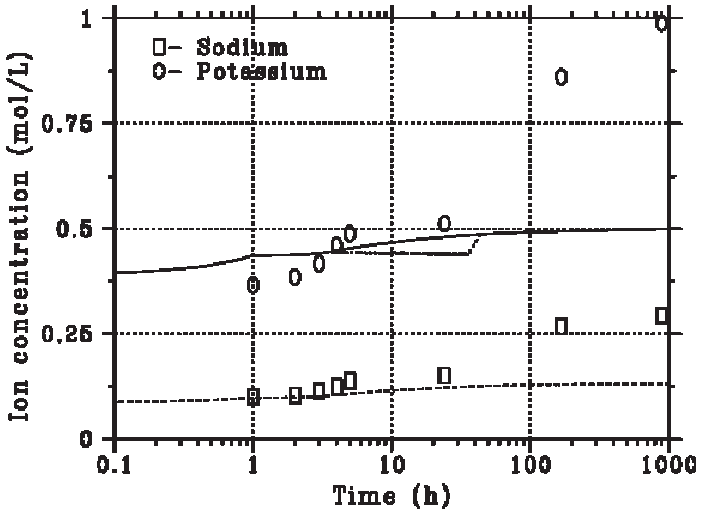

Figure 10

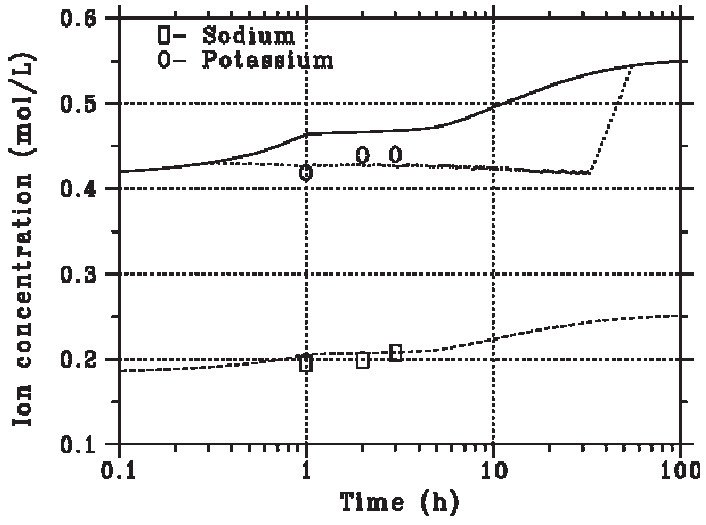

Figure 11

Mortar Cube Compressive Strength Development

The predicted and measured compressive strength development for ASTM C109 mortar cubes /1/ is provided in Figure 12. The prefactors used in applying Power's gel-space ratio /11/ to compute the model compressive strengths were 96.5 MPa and 83.6 MPa for cements 135 and 141, respectively. While the 3 d strengths are slightly underpredicted and the 28 d strengths are slightly overpredicted, all model predictions are well within 2 standard deviations of the CCRL-determined experimental values. Because 28 d strength is the most often used criteria for concrete acceptance during construction, the ability to adequately predict 28 d compressive strength based on the VCCTL and an earlier age strength measurement (3 d or 7 d) would result in substantial cost and time savings to the construction industry.

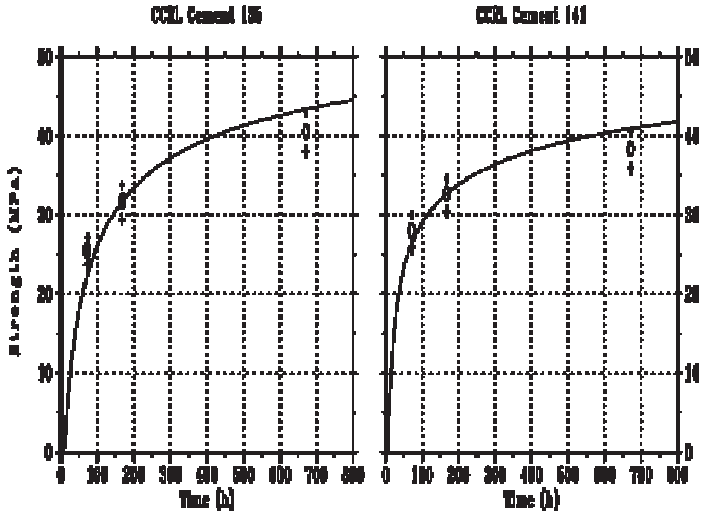

Figure 12

Summary and Prospectus

A wide variety of cement physical properties can be predicted using the VCCTL software. As with any new technology, the cement industry will surely encounter a learning curve in applying the VCCTL in their production and research facilities. However, as indicated by the participation of three cement companies and two major cement associations in the VCCTL consortium, the first steps to perform this integration are well underway.

While this paper has focused on the use of the VCCTL to predict the properties of ordinary portland cements, the VCCTL software is equally applicable to blended cement systems. Silica fume, fly ash, slag, and limestone can all be incorporated into the starting (blended) cement paste microstructures. In this regard, the VCCTL has already been applied to demonstrate the potential of replacing the coarser cement particles by limestone fillers in low w/c ratio high-performance concretes, to reduce costs without sacrificing performance /20/. Current research efforts in the VCCTL consortium are focused on predicting the rheological and elastic properties of cement-based systems, which will further

increase the applicability of the VCCTL to a large number of problems of practical significance. As transport (diffusion) coefficients can already be accurately predicted in the VCCTL, these new developments will provide the foundation for addressing the critical problem of concrete service life prediction and life cycle cost analysis, on a sound materials science-based footing.

Acknowledgements

The authors would like to thank Mr. Robin Haupt of the CCRL for supplying the samples of cements 135 and 141.

References

[1] ASTM Annual Book of Standards, Vol. 04.01 Cement; Lime; Gypsum (American Society for Testing and Materials, West Conshohocken, PA) 1999.

[2] DIN EN 196: Pruefverfahren fuer Zement. (Deutsches Institut fuer Normung e.V., Berlin) 1990-1995.

[3] Bentz, D.P., Forney, G.F.: User's Guide to the NIST Virtual Cement and Concrete Testing Laboratory, Version 1.0. NISTIR 6583, U.S. Department of Commerce, November, 2000.

[4] Cement and Concrete Reference Laboratory Proficiency Sample Program: Final Report on Portland Cement Proficiency Samples Number 135 and Number 136, Cement and Concrete Reference Laboratory, Gaithersburg, MD, March 2000.

[5] Cement and Concrete Reference Laboratory Proficiency Sample Program: Final Report on Portland Cement Proficiency Samples Number 141 and Number 142, Cement and Concrete Reference Laboratory, Gaithersburg, MD, September 2001.

[6] Bentz, D.P., Stutzman, P.E.: SEM Analysis and Computer Modelling of Hydration of Portland Cement Particles. in Petrography of Cementitious Materials, edited by S.M. DeHayes and D. Stark (ASTM, Philadelphia, PA, 1994) p. 60.

[7] Bentz, D.P., Stutzman, P.E., Haecker, C.J., Remond, S.: SEM/X-ray Imaging of Cement-Based Materials, in Proceedings of the 7th Euroseminar on Microscopy Applied to Building Materials, Eds. H.S. Pietersen, J.A. Larbi, and H.H.A. Janssen, Delft University of

Technology, pp. 457-466 (1999), available online at http://ciks.cbt.nist.gov/bentz/eurosem/semcolor.html.

[8] Castleman, K.R.: Digital Image Processing.(Prentice-Hall, Englewood Cliffs, NJ, 1979).

[9] Bentz, D.P.: Three-Dimensional Computer Simulation of Portland Cement Hydration and Microstructure Development. *Journal of the American Ceramic Society*, 80 (1), 3-21, 1997.

[10] Bentz, D.P.: CEMHYD3D: A Three-Dimensional Cement Hydration and Microstructure Development Modelling Package. Version 2.0. NISTIR 6485, U.S. Department of Commerce, April 2000, available online at http://ciks.cbt.nist.gov/bentz/cemhyd3dv20.

[11] Taylor, H.F.W., Cement Chemistry (Thomas Telford, London, 1997).

[12] Bentz, D.P., Feng, X., Haecker, C.J., Stutzman, P.E.: Analysis of CCRL Proficiency Cements 135 and 136 Using CEMHYD3D. NISTIR 6545, U.S. Department of Commerce, August 2000.

[13] Longuet, P., Burglen, L., Zelwer, A. *Revue Materiaux et Constructions*, 35, 1973.

[14] Geiker, M.: Studies of Portland Cement Hydration: Measurement of Chemical Shrinkage and a Systematic Evaluation of Hydration Curves by Means of the Dispersion Model. Ph. D. thesis, Technical University of Denmark, Lyngby, Denmark, 1983.

[15]Powers, T.C.: Adsorption of Water by Portland Cement Paste during the Hardening Process. *Industrial and Engineering Chemistry*, 27, 790-794, 1935.

[16] Taylor, B.N., Kuyatt, C.E.: Guidelines for Evaluating and Expressing the Uncertainty of NIST Measurement Results. NIST Technical Note No. 1297, U.S. Department of Commerce, Washington, D.C., Sept. 1994.

[17] Burrows, R.W., Kepler, W.F., Hurcomb, D., Schaffer, J., Sellers, G.: Three Simple Tests for Selecting Low-Crack Cement. to appear in *Cement and Concrete Composites*, November 2002.

[18] Snyder, K.A., Feng, X., Keen, B., Mason, T.O.: Estimating the Electrical Conductivity of Cement Paste Pore Solutions from K^+ and Na^+ Concentrations. submitted to *Cement and Concrete Research*, 2002.

[19] Gartner, E.M., Tang, F.J., Weiss, S.J.: Saturation Factors for Calcium Hydroxide and Calcium Sulfates in Fresh Portland Cement Pastes. *Journal of the American Ceramic Society*, 68 (12), 667-673, 1985.

[20] Bentz, D.P., Conway, J.T.: Computer Modelling of the Replacement of “Coarse” Cement Particles by Inert Fillers in Low w/c Ratio Concretes: Hydration and Strength. *Cement and Concrete Research*, 31 (3), 503-506, 2001.